On measurement of dislocation core distributions in GaAs/ZnTe/CdTe heterostructure by transmission electron microscopy

Sławomir Kret†, Paweł Dłużewski ‡, Piotr Dłużewski† and Jean-Yves Laval§

† Institute of Physics, PAS, Al. Lotników 32/46, 02-668 Warszawa

‡ Institute of Fundamental Technological Research, PAS,

ul.Świętokrzyska 21, 02-049 Warszawa

§ Laboratoire de Physique du Solide - E.S.P.C.I. CNRS UPR 05,

10 rue Vauquelin, 75231 Paris cedex 05

June 19, 2002

Abstract

Tensorial maps of misfit dislocations at the strained GaAs/ZnTe/CdTe interfacial zone are reconstructed by use of digital processing of High Resolution Transmission Electron Microscopy (HRTEM) micrographs. Large distortions of the crystal lattice around Lomer dislocations are measured using the geometric phase technique. The integration of the dislocation distribution tensor field over a dislocation core region gives the in-plane components of their Burgers vectors. The accuracy of the method for the dislocation map reconstruction is tested by comparing the theoretical values of the so-called true Burgers vectors with those obtained from the integration of tensorial maps.

1 Introduction

In recent years, several papers have been devoted to the measurement of lattice distortions from the HRTEM micrographs – particularly in the case of semiconductor pseudomorphic layers or coherent islands. (Bayle *et al.* 1993; Bierwolf *et al.* 1993; Robertson *et al.* 1995; Kret *et al.* 1998; Hÿtch *et al.* 1998; Snoeck *et al.* 1998). It was based on the assumption of a direct relationship between the intensity maxima in HRTEM images and the atomic columns position in the observed samples. The maxima positions were precisely determined by use of the respective image processing routines. The positions in experimental lattice were compared with those calculated on the basis of the distances measured in a perfect crystal near the analysed area. Next the displacement fields were determined as displacement vector between corresponding nodes of deformed and reference lattices. Another technique called the geometric phase method has been developed by Hÿtch *et al.* (1998). This technique is more convenient than the method mentioned above for the measurement of lattice distortions in faulted regions, e.g. around dislocations because, in contrary to peak finding procedure, the numbering of the lattice points in reference and actual configuration are not necessary. This approach has been used by Snoeck *et al.* (1998) to measure the lattice distortion in vicinity of misfit dislocations situated at the interface in heteroepitaxial GaAs/GaSb. Mbus and Wagner (1999) have used the geometric phase maps to study influence of the delocalisation effect of different types microscopes (field emission, high voltage, Cs corrected) on the measured distortion field near dislocation at Cd/Ni interfaces.

These two methods are not suitable for the determination of atomic structure of dislocation. The more general approaches based on a quantitative comparison between the simulated and experimental images are needed. Mobus (1996) has proposed a method based on an iterative structure retrieval which was successfully applied to analyse the atomic configuration of edge dislocations in niobium. The incoherent imaging technique as Z-contrast was successfully applied to find the atomic structure of misfit dislocations in CdTe/GaAs(100) by Mc Gibbon *et al.* (1995).

In the following, an approach based on the continuum field theory is employed to digital image processing and the distribution of dislocation cores are extracted from HRTEM micrographs.

Due to strong lattice distortions near the defects cores, we used the mathematical theory of dislocations based on so-called large deformation approach in which the differences between the reference lattice

(undeformed) and the actual configuration of the crystal lattice are considered. In particular, our method relates to the idea of the description of the dislocated crystal lattice in terms of the nonlinear theory of large elastic-plastic deformations (cf. Teodosiu 1970; Kröner 1981; Dłużewski 1996).

2 Experimental details

HRTEM images of GaAs/ZnTe/CdTe heterointerface along the [110] zone axis are used to demonstrate the dislocation core measurement (Fig.1).

[Insert figure 1 here]

A thick CdTe film was grown by molecular beam epitaxy (MBE) on GaAs (100) 2° misoriented substrate. Before growth, the surface oxide was removed by flash heating of the substrate in an ultra-high vacuum chamber in a Te flux. A thin, 20-60nm thick, ZnTe intermediate layer seems to be the best way for obtaining high quality CdTe {100} layers (Tatarenko *et al.* 1989), but in our case, the growth was started by deposing 2 monolayers of ZnTe on GaAs substrate followed by CdTe to obtain a buffer layer used to grow quantum structures. The growth process was performed at 350°C at a $1\,\mu$/h growth rate. The {110} cross-sectional specimens were prepared using the conventional grinding and ion beam thinning with liquid nitrogen cooling. The high resolution electron microscopy was performed by using a Philips CM 20 UT microscope operating at 200 kV with a point resolution of 0.19 nm. For HRTEM observation an aperture of 11 nm^{-1} (including 9 beams: $000, 4 \times 111, 2 \times 220, 2 \times 200$) was used for image formation. The thickness of the foil for which the images were analysed was uniform and estimated to be below 15 nm. Simulated images of GaAs and CdTe crystals along the [110] zone axis show that close to Scherzer defocus and foil thicknesses between 5 and 15 nm the bi-atomic column positions are represented by white dots. In practice, the defocus value was slightly tuned to keep homogeneous contrast (with bright dots on a dark background) for GaAs and CdTe crystal in the whole-observed area. The images were recorded on photographic plates and digitized with a resolution of 3 pixels/Å and 8 bits dynamic. A typical high quality image of GaAs/CdTe interface along the [110] projection is shown in Fig. 1. The interface (substrate surface) was tilted about 2° relatively to [100] crystallographic direction, so 4 mono-atomic steps appear between the left and right borders of the image.

Their probable positions have been marked by horizontal line segments in fig. 1. A network of dislocations at the interface accommodates most of the 14.6

The tilt of the CdTe lattice relatively to the substrate is less than 1° in the analyzed area, which is small compared with the 6° reported by Cheng *et al.* (1995), for growth of CdTe directly on GaAs substrate. Nine of the ten misfit dislocations visible on the interface are edge Lomer dislocations. Their Burgers vectors have components $\frac{1}{2}[1\bar{1}0]$. The dislocation lines are parallel to the interfacial plane and to the electron beam. Only one 60° dislocation is visible at the interface (see dislocation no. 10). The second 60° dislocation is situated at 8 nm from the interface (dislocation n^o 11). Other dislocations (not shown in Fig 1) were found far away from the interface at 20-25nm. Burgers vector of this kinds of dislocation has components $\frac{1}{2}[0\bar{1}\bar{1}]$ or $\frac{1}{2}[10\bar{1}]$ and is deviated by 60° from the dislocation line being parallel to the electron beam and is laying in $(1\bar{1}1)$ plane. The image pattern of all dislocations visible in Fig. 1 are different from one to the next.

We will demonstrate that by using a self-consistent digital processing of HRTEM images in properly chosen conditions, the lattice distortion field and the dislocation core distribution can be correctly extracted from HRTEM images. In the next section, we briefly summarised the theoretical foundations of the nonlinear continuum mechanics which have been employed in this work.

3 Relations between the deformation and displacement fields

By a continuum we mean an open set in the three dimensional oriented Euclidean space E^3. Let $\mathbf{X}$ denote the reference position of a material element which after deformation takes a new position $\mathbf{x}$, see Fig.2. Limiting our considerations to orthonormal coordinate systems in E^3, the coordinates x_k and X_K of the material element occupying the initial and current positions $\mathbf{x}$ and $\mathbf{X}$ can be treated as components of the respective vectors. In such a case the displacement vector is determined as the following difference :

$$\mathbf{u} = \mathbf{x} - \mathbf{X} \tag{1}$$

The gradient of the displacement vector field $\mathbf{u}(\mathbf{x})$ is defined as:

$$\nabla \mathbf{u} \stackrel{df}{=} \frac{\partial \mathbf{u}}{\partial \mathbf{x}} = \frac{\partial \mathbf{u}}{\partial \mathbf{X}} \frac{\partial \mathbf{X}}{\partial \mathbf{x}} \tag{2}$$

Alternatively, the deformation of the body can be described by the mapping $\mathbf{x} = \mathbf{x}(\mathbf{X})$. A deformation gradient $\mathbf{F}$ is defined as a generally nonsymmetric tensor :

$$\mathbf{F} \stackrel{df}{=} \frac{\partial \mathbf{x}}{\partial \mathbf{X}} \tag{3}$$

The description based on the mapping $\mathbf{x}(\mathbf{X})$ is found to be more general than the approach based upon the displacement field $\mathbf{u}(\mathbf{x})$. This concerns mainly non-Euclidean spaces where, with respect to the space curvature, the displacement vector fields can not be used to determine the lattice displacements. In the next section it will be shown how the lattice displacements in E^3 can be described by using the piecewise continuous displacement fields where the segments are separated by discontinuity lines. Substituting (1) and (3) into (2) we find a reversible relation between $\nabla\mathbf{u}$ and $\mathbf{F}$

$$\nabla\mathbf{u} = \mathbf{1} - \mathbf{F}^{-1} \qquad \text{and} \qquad \mathbf{F} = (\mathbf{1} - \nabla\mathbf{u})^{-1} \tag{4}$$

[Insert figure 2 about here]

3.1 Dislocated crystal lattice

We present here the fundamental relations of the continuum theory of dislocations , see Kröner (1958); Kröner (1981); Teodosiu (1970, 1982); Gairola (1979); Dłużewski (1996). To take into account the difference between the total and lattice deformations it is convenient to decompose the total deformation gradient $\mathbf{F}$ into the lattice deformation tensor $\mathbf{F}_{\mathrm{lt}}$ and a remnant $\mathbf{F}_{\mathrm{pl}}$ induced by the process of rebuilding of the crystal lattice during plastic deformation).

$$\mathbf{F} = \mathbf{F}_{\mathrm{lt}}\mathbf{F}_{\mathrm{pl}} \tag{5}$$

Apart from the displacement field $\mathbf{u}(\mathbf{x})$ describing the displacements of mass , cf. (2), we can determine a second field corresponding to local displacements of lattice points $\widehat{\mathbf{u}}(\mathbf{x})$ the current to the lattice reference configuration identified with an arbitrarily chosen region in a perfect lattice structure, see fig. 2.

The first field corresponds to the total deformation induced both by plastic (rebuilding) and elastic deformations, while the second one corresponds only to a local elastic unloading to the nearest atomic position

in a perfect lattice. In result, the first one is continuous and satisfies so-called compatibility conditions while the second gives discontinuity lines departing from dislocation cores.

$$\widehat{\mathbf{u}} = \mathbf{x} - \widehat{\mathbf{x}} \tag{6}$$

such that

$$\boldsymbol{\beta} = \frac{\partial \widehat{\mathbf{u}}}{\partial \mathbf{x}} \qquad \text{and} \qquad \mathbf{F}_{\mathrm{lt}} = \frac{\partial \mathbf{x}}{\partial \widehat{\mathbf{x}}} \tag{7}$$

Similarly as in the case of distortions $\nabla \mathbf{u}$ in a perfect lattice, we find, cf. (4),

$$\boldsymbol{\beta} = \mathbf{1} - \mathbf{F}_{\mathrm{lt}}^{-1} \qquad \text{and} \qquad \mathbf{F}_{\mathrm{lt}} = (\mathbf{1} - \boldsymbol{\beta})^{-1} \tag{8}$$

The fundamental difference in relation to the total distortion measures discussed previously lies in the so-called compatibility conditions. For a dislocated crystal lattice we are not able to determine a continuous lattice displacement field without lattice rebuilding which could relax the lattice, as a whole, back to the perfect lattice. From the mathematical point of view, the necessary condition to find such a continuous displacement field $\widehat{\mathbf{u}}(\mathbf{x})$ relating of the deformed lattice to the perfect one takes the form

$$\bigwedge_{\mathbf{x} \in V_{\mathrm{cr}}} \operatorname{curl} \boldsymbol{\beta} = \mathbf{0} \tag{9}$$

where $\bigwedge_{\mathbf{x} \in V_{\mathrm{cr}}}$ reads for all $\mathbf{x}$ in the whole crystal volume region. In the index notation the operator $\operatorname{curl} \boldsymbol{\beta}$ reads $\frac{\partial \beta_{ij}}{\partial z_k} e_{jkl} = 0$, where e_{jkl} is the permutation symbol, cf. (18). In other words, if the above condition is satisfied, then for a given four-component field $\boldsymbol{\beta}(\mathbf{x})$ there will exist a two-component vector field $\mathbf{u}(\mathbf{x})$ such that $\boldsymbol{\beta}(\mathbf{x}) = \nabla \mathbf{u}$. Obviously, in a general case, for an arbitrary chosen four-component field $\beta_{11}(\mathbf{x}), \beta_{12}(\mathbf{x}), \beta_{21}(\mathbf{x}), \beta_{22}(\mathbf{x})$ we are not able to find only two-component field $u_1(\mathbf{x}), u_2(\mathbf{x})$ which could generate four mutually different component fields of distortions. The necessary condition for integrability of $\boldsymbol{\beta}(\mathbf{x})$ to obtain a continuous $\mathbf{u}(\mathbf{x})$ takes the form (9).

3.2 Distribution of the true Burgers vectors

Two Burgers vectors are associated with a given dislocation (Hirth and Lothe (1982)). The so-called true Burgers vector refers to the interatomic distances in a perfect crystal lattice, while the *local* Burgers vector

is measured in relation to the lattice spacing in the studied area in which the dislocation is observed. These two vectors are different. Analogously, in the continuum theory of dislocations a few mutually different tensorial measurements of dislocation distribution are introduced, cf. (10) and (21). The distribution of the true Burgers vector is described by the following dislocation distribution tensor

$$\widetilde{\boldsymbol{\alpha}} \stackrel{df}{=} \operatorname{curl} \mathbf{F}_{\mathrm{lt}}^{-1} = \quad -\operatorname{curl} \boldsymbol{\beta} \tag{10}$$

In the subscript notation this means that

$$\widetilde{\alpha}_{ik} = -\frac{\partial \beta_{im}}{\partial x_n} e_{mnk} \tag{11}$$

Let the Burgers circcuit be drawn around the dislocation core in the studied configuration. Making a local mapping to any chosen reference configuration of the perfect lattice we find the respective unclosed circuit $\widehat{c}$ in the reference configuration, see figure 2. The vector $\widehat{\mathbf{b}}$ needed to close the circuit is called the true Burgers vector. Using the Stokes theorem this local mapping takes the following mathematical representation in the continuum theory of dislocations

$$\widehat{\mathbf{b}} = \oint_c \frac{\partial \widehat{\mathbf{x}}}{\partial \mathbf{x}} d\mathbf{x} = \oint_c \mathbf{F}_{\mathrm{lt}}^{-1} d\mathbf{x} = \int_{s_c} \widetilde{\boldsymbol{\alpha}}\, ds \tag{12}$$

where s_c is the region occupied by dislocation core in the actual configuration. The differential $d\mathbf{s}$ is understood here as a product $d\mathbf{s} = \mathbf{n}\, ds$ where $\mathbf{n}$ is the unit vector perpendicular to the cross-section, while ds is a scalar area element of dislocation core. The geometric meaning of the tensorial measure $\widetilde{\boldsymbol{\alpha}}$ can be also expressed in a differential form :

$$d\widehat{\mathbf{b}} = \widetilde{\boldsymbol{\alpha}}\, d\mathbf{s} \tag{13}$$

relating the respective increase of the Burgers vector $d\widehat{\mathbf{b}}$ to the area element $d\mathbf{s}$ of dislocation core region.

The dislocation core distribution $\widetilde{\boldsymbol{\alpha}}(\mathbf{x})$ is particularly interesting in the case of the dislocation which can be dissociated. For example, for Lomer dislocation the splitting of elemental 60 dislocations will be clearly visible in distribution of $\widetilde{\boldsymbol{\alpha}}(\mathbf{x})$

4 Practical image processing and results

Our procedure for measuring dislocation distribution starts with the reconstruction of distortion fields from HRTEM micrograph. The geometric phase method is suitable to analyse distortions in a strongly dislocated materials. In our case, 1024x1024 pixels HRTEM images have been recorded (Fig.1). The unit vectors $\mathbf{e}_1, \mathbf{e}_2, \mathbf{e}_3$ composing the vector basis in the orthonormal coordinate system $\{x_k\}$ has been chosen as follows

$$\begin{aligned} \mathbf{e}_1 &= \tfrac{1}{\sqrt{2}}[1\bar{1}0] \quad \text{– horizontal direction} \\ \mathbf{e}_2 &= [00\bar{1}] \quad \text{– vertical direction} \\ \mathbf{e}_3 &= \tfrac{1}{\sqrt{2}}[110] \quad \text{– electron beam dir.} \end{aligned} \tag{14}$$

The phase images $P_{\mathbf{g}_{\bar{1}\bar{1}1}}(x_1, x_2)$ and $P_{\mathbf{g}_{1\bar{1}1}}(x_1, x_2)$, shown in fig. 3, were obtained by applying circular masks around $[1\bar{1}\bar{1}]$ and $[1\bar{1}1]$ Bragg peaks, cf. Fig. 1. The dislocations free GaAs substrate structure was chosen as a reference configuration, see geometric phase method Hÿtch *et al.* (1998). The image processing was performed with the program written using OPTIMAS Analytical Language for Images (Media Cybernettics 1999).

Figure 3 shows a abrupt change of the geometric phase from 0 to 2π in the CdTe crystal area and the discontinuity lines point out the position of missing CdTe (111) planes. In GaAs substrate area the small phase variation from 0 to 0.5π is observed in the $\mathbf{e}_1$ direction. This variation is due to a slight variation of imaging conditions from right to left of the image. This long range geometric phase gradient is negligible in CdTe layer where the phases changes from 0 to 2π on the distance between dislocations.

[Insert figure 3 here]

The lattice displacement $\widehat{\mathbf{u}}(\mathbf{x})$,where $\mathbf{x} = x_1\mathbf{e}_1 + x_2\mathbf{e}_2$, has been calculated using the following formula, see Hÿtch *et al.* (1998):

$$P_{\mathbf{g}_i}(\mathbf{x}) = -2\pi \mathbf{g}_i \cdot \widehat{\mathbf{u}}(\mathbf{x}) \tag{15}$$

which can be rewritten for vectors $\mathbf{g}_1$ and $\mathbf{g}_2$ as follows :

$$\begin{aligned} P_{\mathbf{g}_1}(\mathbf{x}) &= -2\pi \mathbf{g}_1 \cdot \widehat{\mathbf{u}}(\mathbf{x}) = -2\pi \left(g_{1_1} \widehat{u}_1(\mathbf{x}) + g_{1_2} \widehat{u}_2(\mathbf{x}) \right) \\ P_{\mathbf{g}_2}(\mathbf{x}) &= -2\pi \mathbf{g}_2 \cdot \widehat{\mathbf{u}}(\mathbf{x}) = -2\pi \left(g_{2_1} \widehat{u}_1(\mathbf{x}) + g_{2_2} \widehat{u}_2(\mathbf{x}) \right) \end{aligned} \tag{16}$$

The two-dimensional distortion field $\boldsymbol{\beta}(\mathbf{x})$ shown in Fig. 4 is obtained by differentiation of the displacement field $\widehat{\mathbf{u}}(\mathbf{x})$ according to (7). The distortions have been determined using the following equation :

$$[\boldsymbol{\beta}] = \begin{bmatrix} \beta_{11} & \beta_{12} \\ \beta_{21} & \beta_{11} \end{bmatrix} = \begin{bmatrix} \frac{\partial \widehat{u}_1}{\partial x_1} & \frac{\partial \widehat{u}_1}{\partial x_2} \\ \frac{\partial \widehat{u}_2}{\partial x_1} & \frac{\partial \widehat{u}_2}{\partial x_2} \end{bmatrix} \tag{17}$$

The displacement discontinuity cause to undetermined distortion lines on a continuous distortion field. From the numerical point of view, the undetermined regions were occupied by 1-2 sequential pixels only. Due to the continuous character of the distortion field, the undetermined values on the discontinuity lines were easy retrieved by interpolation. In the dislocation centres we obtained always a few neighbours pixels with very high negative and positive values up to $\beta_{ij} = \pm 105$, but in the mentioned region the components of $\boldsymbol{\beta}(\mathbf{x})$ change the sign in a continuous way. Therefore, all pixels with "artificial" values of $\boldsymbol{\beta}(\mathbf{x})$ were removed by applying the symmetric cut off to $\boldsymbol{\beta}(\mathbf{x}) = \pm 0.75$ and all missing pixels was restored using a bi-quadratic interpolation function. The performed test shows that the threshold value and interpolation function applied are not critical for calculated Burgers vector, which can be obtained with high precision practically independently of this parameters.

[Insert figure 4 about here]

The field $\boldsymbol{\beta}(\mathbf{x})$ determined in relation to the GaAs reference substrate is shown in Fig 3. In the case of dislocations $1, 4, 7, 8$, the dissociation of dislocation cores into elemental 60° dislocations is clearly visible. Due to over two times larger stiffness of GaAs than CdTe the elastic field disturbance induced by interfacial dislocations is weaker in GaAs. It is clearly visible on the maps of β_{11} and β_{22}.

The components of dislocation distribution tensor, α_{12} and α_{23}, have been determined by means of (11) using the field $\boldsymbol{\beta}(\mathbf{x})$. All non-vanishing components of the alternating tensor e_{ijk} were limited to $e_{123} = +1$ and $e_{213} = -1$, which leads to the following index relations :

$$\begin{aligned} \widetilde{\alpha}_{13} = -\beta_{1i,j}\, e_{ij3} &= -\beta_{12,1} + \beta_{11,2} = -\frac{\partial \beta_{12}}{\partial x_1} + \frac{\partial \beta_{11}}{\partial x_2} \\ \widetilde{\alpha}_{23} = -\beta_{2i,j}\, e_{ij3} &= -\beta_{22,1} + \beta_{21,2} = -\frac{\partial \beta_{22}}{\partial x_1} + \frac{\partial \beta_{21}}{\partial x_2} \end{aligned} \tag{18}$$

Such determined plane components of tensorial field of dislocation distribution take zero value in the whole analysed region excepting the dislocation cores where they form the characteristic local peaks, see Fig. 5.

The size and shape of peaks depend on the interpolation procedure applied (bi-quadratic interpolation). The peaks are surrounded by zero value field with the accuracy 10^{-6} of the densities values reached at the peaks even at the retrieved pixels on the discontinuity lines, which confirms the validity of the interpolation methods used to recover missing pixels. The dislocation density tensor determines uniquely the Burgers vector. Integrating the components $\widetilde{\boldsymbol{\alpha}}$ over the whole dislocation core region, we can find the components of the so-called true Burgers vectors. According to (12) we find

$$\begin{aligned} \widehat{b}_1 &= \int_{S_c} \widetilde{\alpha}_{13} n_3 ds \approx \sum_{i=1}^{k} \widetilde{\alpha}_{13} \Delta S_{\mathrm{pxl}_i} \\ \widehat{b}_2 &= \int_{S_c} \widetilde{\alpha}_{23} n_3 ds \approx \sum_{i=1}^{k} \widetilde{\alpha}_{23} \Delta S_{\mathrm{pxl}_i} \end{aligned} \tag{19}$$

where S_{pxl_i} denotes the area occupied by i-th pixel. In digital image processing the whole dislocation core has been divided into element area corresponding to pixels, i.e. $S_{\mathrm{pcl}_i} = \sum_{i=1}^{k} \Delta S_{\mathrm{pxl}_i}$. In our case, the dislocation distribution tensor has been rescaled to : $\mathbf{f}(\mathbf{x}) = \widetilde{\boldsymbol{\alpha}}(\mathbf{x}) \Delta S_{pxl}$. The plane components of the Burgers vector of the analysed dislocation can be simply calculated in a rectangle surrounding a given dislocation core. From practical point of view, in this frame the resulting values were nothing else that the sum of the values reached by $\mathbf{f}(\mathbf{x})$ in the marked area, cf. green rectangles marked in figure 5, and the resulting values of components of the Burgers vectors, ie. $\widehat{\mathbf{b}} = \sum_i \mathbf{f}(\mathbf{x}_i)$.

The results of integration as well as the dislocation core distribution field obtained here are shown in figure 5.

We tested different interpolation functions as well as different cutting levels for discontinuity removing and the final values of Burgers vectors was always the same as shown in Tab. 1 (precision 0.01 [$\mathring{A}$]). So, the calculated Burgers vectors do not depend of the interpolation procedure applied. Since, as in the Burgers method, the exact values of the Burgers vector compounds are determined uniquely by the environment of the defect, where the Burgers circuit is drawn.

The upper row of pictures in Fig.5 presents the enlarged fragments of image shown in Fig. 1. The following rows of pictures show the contour plots of dislocation core density components $\widetilde{\alpha}_{13}$ and $\widetilde{\alpha}_{23}$ for marked square frames shown on upper images. It is clearly visible that the dislocation core density tensor takes non zero values only near a dislocation center in a radius of about 0.5 nm.

Note, that for the considered heterostructure, we can assume many different reference lattices. For

example, instead of a perfect lattice shown in the lower image in figure 1-20 on page 22 in Hirth and Lothe (1982) we could assume here a perfect CdTe structure as the reference one, then the different true Burgers vectors could be determined. Obviously, the most convenient reference structure seems to be the one based upon the real chemical composition of given crystal zone. However, the problem is that in the transient interfacial zone the real composition is often difficult to determine, especially in the vicinity of dislocation cores. Moreover, to compare the tensorial fields obtained for different dislocations situated in one heterostructure, it is convenient to take a common reference lattice. In our particular case we have referred the Burgers vectors of all dislocations to the perfect GaAs lattice according to the FS/RH method. Therefore, even for dislocation no 11 situated in the CdTe lattice we have obtained the true Burgers vector whose components reach values proper to the perfect lattice assumed as the reference one (GaAs).

Dislocations 4 and 5 have the same true Burgers vector but their tensorial maps are quite different. Dislocations 3, 4 and 7 have clearly visible double peaks of $\widetilde{\alpha}_{13}$ with maximum value 0.022 $[\mathring{A}]$/pix but the field $\widetilde{\alpha}_{23}$ is split to maximum and minimum. Integrating separately the two partial dislocations, we obtain two Burgers vectors corresponding to in-plane components of two opposite 60° dislocations . However it is also possible that this peak separation results from an the symmetry breaking of the distortion fields $\boldsymbol{\beta}$ around core. For a perfect dislocation with a dislocation line parallel to the e-beam the shape of the "wings" of $\boldsymbol{\beta}$ distribution must have regular, symmetric character. After calculation, this gives a single peak α . If the dislocation is dissociated, the measured distortion field consists of two superimposed distortion fields generated by two elementary dislocations. But splitting can also occur if the dislocation line is not parallel to the zone axis, for example due to local foil skewing or presence of steps on the GaAs substrate invisible due to projection (dislocation line can change position through the foil thickness).

Other possible explanation can arise from the variation of imaging parameters like thickness and defocus, but in our case, the dislocations are very close to each other and it is difficult to expect large variation of the imaging parameters on these short distances. However, the influence of experimental condition must be better understood and the appropriate simulations are scheduled in future works. The possible origin of the α peaks splitting is the instability of the core structure in this complex material system. As an example, an unexpected atomic configuration of dislocation cores was found in the GaAs/CdTe interface by Z contrast

investigation by McGibbon et al.1996. However, future analyses will be necessary to correlate the observed origin of the α distribution variation versus the atomic structure of cores.

Summarising, on the basis of the α distribution extracted from fig 1, we can distinguish a perfect Lomer dislocation (5) and a highly dissociated Lomer dislocation (1,7,8). The splitting of the α peaks for the remaining dislocations (2,3,4,5,6,9), which are interpreted as the Lomer dislocations, can also results from the reason discussed above.

The proposed procedure gave the Burgers vectors related to the lattice constant in the reference material independently of the variety of shapes of α field.

[Insert figure 5 about here]

5 Local Burgers vectors

In section 3.2, using the geometric phase technique on HRTEM images , the true Burgers vectors of dislocations have been determined. Starting from local mappings of a heterostructure GaAs/ZnTe/CdTe into the GaAs reference structure we determined step by step:

1. a piecewise continuous lattice displacement field $\widehat{\mathbf{u}}$,
2. continuous lattice distortion fields $\boldsymbol{\beta}$ and $\mathbf{F}_{\mathrm{lt}}$, cf. (8) and (7),
3. continuous dislocation distribution field $\widetilde{\boldsymbol{\alpha}}$, cf. (10b).

For example, integrating of $\widetilde{\boldsymbol{\alpha}}$ over the core region of dislocation no 11 situated in CdTe we have found the true Burgers vector, 1/2<110>. However, the measured components do not correspond to a strongly deformed CdTe structure but are 14% smaller, and correspond to the reference GaAs structure, for which the distortion $\mathbf{F}_{\mathrm{lt}}$ and $\boldsymbol{\beta}$ have been determined previously. So, calculated in this way Burgers vectors have a value corresponding to the undeformed lattice $\frac{\sqrt{2}}{2}a_{\mathrm{GaAs}}$ instead of $\frac{\sqrt{2}}{2}a_{\mathrm{CdTe}}$, — in spite of the integration being carried out over the cross-section in CdTe (cf. the result of integration shown in Fig. 5 for dislocation no 11). To avoid such discrepancies, in the dislocation theory, two Burgers vectors are assigned for every dislocation (see SF/RH Burgers circuit shown in figure 1-21 by Hirth and Lothe (1982). Note, that the difference between

the values of the true and local Burgers vectors is usually negligible because the elastic deformation of given crystal lattice is very small. But in heterostructures composed of quite different materials the difference takes a significant level due to different equilibrium lattice constants (chemical distortion). For example, in our case for dislocation 11 the difference exceeds 14%.

In the dislocation theory, the local Burgers vectors can be found by using the transformation rule for differentials of the Burgers vector from the reference to the actual configuration, $d\mathbf{b} = \mathbf{F}_{\mathrm{lt}} d\widehat{\mathbf{b}}$, we find

$$d\mathbf{b} = \mathbf{F}_{\mathrm{lt}} \widetilde{\boldsymbol{\alpha}} d\mathbf{s} = \boldsymbol{\alpha} d\mathbf{s} \tag{20}$$

cf. (13), where the spatial distribution of the local Burgers vector is defined as

$$\boldsymbol{\alpha} \overset{df}{=} \mathbf{F}_{\mathrm{lt}} \operatorname{curl} \mathbf{F}_{\mathrm{lt}}^{-1} = -(\mathbf{1} - \boldsymbol{\beta})^{-1} \operatorname{curl} \boldsymbol{\beta} \tag{21}$$

In the index notation the last equation reads $\alpha_{ik} = -(1-\beta)^{-1}_{ij} \frac{\partial \beta_{jm}}{\partial x_n} e_{mnk}$.

The definition of $\boldsymbol{\alpha}$ means that integrating $\boldsymbol{\alpha}$ over the cross-section of dislocation core in the actual configuration we can obtain the local Burgers vector $\mathbf{b}$ from the same configuration, cf. (12),

$$\mathbf{b} = \int_{s_c} \boldsymbol{\alpha} d\mathbf{s} \tag{22}$$

Both of the Burgers vectors $\mathbf{b}$ and $\widehat{\mathbf{b}}$ are widely used in dislocation theory. In heterostructures where the lattice deformation is often very large due to a change in chemistry, the difference between the actual and lattice reference configurations becomes considerable. Calculating components of α_{13} and α_{23} from (21), we find

$$\begin{aligned} \alpha_{13} &= \left[(\mathbf{1} - \boldsymbol{\beta})^{-1}\right]_{11} \widetilde{\alpha}_{13} + \left[(\mathbf{1} - \boldsymbol{\beta})^{-1}\right]_{12} \widetilde{\alpha}_{23} \\ \alpha_{23} &= \left[(\mathbf{1} - \boldsymbol{\beta})^{-1}\right]_{21} \widetilde{\alpha}_{13} + \left[(\mathbf{1} - \boldsymbol{\beta})^{-1}\right]_{22} \widetilde{\alpha}_{23} \end{aligned} \tag{23}$$

where for two-dimensional tensorial fields rewritten in orthogonal coordinates, the components of the tensor inverse to $\mathbf{1} - \boldsymbol{\beta}$ is given by:

$$(\mathbf{1} - \boldsymbol{\beta})^{-1} = \begin{bmatrix} \frac{1-\beta_{22}}{\det(\mathbf{1}-\boldsymbol{\beta})} & \frac{-\beta_{12}}{\det(\mathbf{1}-\boldsymbol{\beta})} \\ \frac{-\beta_{21}}{\det(\mathbf{1}-\boldsymbol{\beta})} & \frac{1-\beta_{22}}{\det(\mathbf{1}-\boldsymbol{\beta})} \end{bmatrix} \tag{24}$$

The obtained distribution of α_{13} and α_{23} components are very similar to the previously obtained ones shown in figure 5 for $\widetilde{\alpha}_{13}$ and $\widetilde{\alpha}_{23}$. The in-plane components of the local and true Burgers vectors referring to the

actual and reference configuration are given in Table 1 for all dislocations visible in Fig 1).

[Insert table 1 about here]

The analysis of Table 1 shows that for all dislocations, their Burgers vectors recovered from integration of $\boldsymbol{\alpha}$ in the actual configuration are slightly smaller than the corresponding ones in the perfect CdTe lattice. This may be explained by the misfit stress as well as by a redistribution of Zn atoms leading to $Cd_xZn_{1-x}Te$ compound around dislocation cores.

6 Summary

The continuous tensorial field of defects distribution is convenient for computer aided recognition of the geometric parameters of lattice defects on the basis of HRTEM micrographs. As seen above, the dislocation fields $\widehat{\boldsymbol{\alpha}}(\mathbf{x})$ and $\boldsymbol{\alpha}(\mathbf{x})$ have been scaled in such a way that marking a respective frame surrounding one or more dislocation cores, the in plane components of resulting total Burgers vector were displayed immediately on computer screen . From a practical point of view, the proposed technique allows on-line computer aided recognition of the in plane components of Burgers vectors during HRTEM observations.

The applied method gives a very good accuracy for the determination of Burgers vectors. It is worth emphasizing that outside the dislocation cores, within one Burgers vector length the components of the tensors $\boldsymbol{\alpha}$ and $\widetilde{\boldsymbol{\alpha}}$ reach values 10^{-6} of values in core regions. Moreover, the true Burgers vectors of all dislocations ,determined by the integration of dislocation distribution peaks of $\widetilde{\boldsymbol{\alpha}}$ are identical within 0.01 $[\mathring{A}]$, (cf. the column for reference configuration in table 1). So good accuracy is obtained for Burgers vectors; and moreover, zero values taken by $\operatorname{curl}\boldsymbol{\beta}$ outside dislocation cores give a proof of the high reliability to the determined lattice distortion field $\boldsymbol{\beta}(\mathbf{x})$.

7 Acknowledgments

The present work has been partially founded by the State Committee for Scientific Research (KBN) in Poland under Grant No. 7T07A 004 16. The sample has been made in IP-PAS in Warszawa, while the HTREM investigation was carried out on CM-20UT microscope at the Ecole Centrale de Paris. Thanks to

the kind hospitality of Bernard Jouffrey.

References

Bayle, P., Deutsch, T., Gilles, B., Lancon, F., Marty, A. and Thibault, J., 1993, *Ultramicroscopy*, **56**, 94.

Bierwolf, R., Hohenstein, M., Phillipp, F., Brandt, O., Crook, G. E. and Ploog, K., 1993, *Ultramicroscopy*, **49**, 273.

Bonnel, R. and Loubradou, M., 1994, *Physical Review B*, **49**, 14397.

Cheng, T. T., Aindow, M., Jones, I. P., Hails, J. E. and Williams, D. J., 1995, *Journal of Crystal Growth*, **154**, 251.

Dłużewski, P., 1996, *Mechanics of Materials*, **22**, 23.

Gairola, B. K. D., 1979, Nonlinear elastic problems. *Dislocations in Solids*, Vol. 1, edited by F.R.N. Nabaro, p. 223 (Amsterdam: North-Holland).

Hirth, J. P. and Lothe, J., 1982, *Theory of Dislocations* (New York: Wiley). p.752.

Hÿtch, M. J., Snoeck, E. and Kilaas, R., 1998, *Ultramicroscopy*, **74**, 131.

Kret, S., Delamarre, C., Laval, J. Y. and Dubon, A., 1998, *Philosophical Magazine A*, **77**, 249.

Kröner, E., 1958, *Kontinuumstheorie der Vesetzungen und Eigenspannungen.* Springer Verlag, Berlin.

Kröner, E., 1981, *Physics of Defects*, edited by R.Balian, M.Kleman and J.-P. Poiries, (Amsterdam: Nord-Holland) pp. 215–315.

Mc Gibbon, A. J., Pennycook, S. J. and Angelom, J. E., 1995, *Science*, **269**, 519.

Media Cybernettics, Optimas 6.5 User Guide and Technical Reference,1999 .

Mobus, G., 1996, *Ultramicroscopy*, **65**, 205.

Mbus, G. and Wagner, T., 1999, *Journal ofMicroscopy. 194, 1999 p124.* .

Robertson, M. D., Currie, J. E., Corbett, J. M. and Webb, J. B., 1995, *Ultramicroscopy*, **58**, 175.

Snoeck, E., Warot, B., Ardhuin, H., Rocher, A., Casanove, M. J., Kilaas, R. and Hÿtch, M. J., 1998, *Thin Solid Films*, **319**, 157.

Sutton, A.P. and Balluffi R.W. (1995). *Interfaces in Crystalline Materials*. Monographs on the Physics and Chemistry of Materials 51. Oxford University Press.

Tatarenko, S., Cibert, J., Gobil, Y., Feuillet, G., Saminadayar, K., Chami, A. C. and Ligeon, E., 1989, *Applied Surface Science*, **41-42**, 470.

Teodosiu, C., 1970, *Fundamental Aspects of Dislocation Theory*, Nat. Bur. Stand. Spec. Publ., Vol. 317 (2), edited by Simmonds, A. *et al.*, pp. 837–876.

Teodosiu, C., 1982, *Elastic Models of Crystal Defects*. Springer-Verlag and Editura Academiei, Berlin and Bucureşti.

Williams, D. B. and Carter, C. B., 1996, *Transmission Electron Microscopy*. (New York: Plenum Press).

List of Tables

List of Figures

Disl. No	In a perfect GaAs		Lattice reference config.		Actual config.		In a perfect CdTe	
	$\widehat{b}_1$	$\widehat{b}_2$	$\widehat{b}_1$	$\widehat{b}_2$	b_1	b_2	b_1	b_2
1	-3.997	0.0	-4.01	-0.02	-4.54	0.11	-4.583	0.0
2	-3.997	0.0	-4.01	-0.02	-4.51	0.23	-4.583	0.0
3	-3.997	0.0	-4.00	-0.02	-4.43	0.09	-4.583	0.0
4	-3.997	0.0	-4.01	-0.02	-4.21	-0.05	-4.583	0.0
5	-3.997	0.0	-4.01	-0.02	-4.42	-0.04	-4.583	0.0
6	-3.997	0.0	-4.01	-0.02	-4.44	0.28	-4.583	0.0
7	-3.997	0.0	-4.01	-0.02	-4.42	0.00	-4.583	0.0
8	-3.997	0.0	-4.01	-0.02	-4.21	0.07	-4.583	0.0
9	-3.997	0.0	-4.01	-0.02	-4.51	-0.02	-4.583	0.0
10	-1.999	2.818	-2.01	2.83	-2.33	3.13	-2.291	3.241
11	-1.999	-2.818	-2.00	-2.85	-2.54	-3.33	-2.291	-3.241

Table 1: Burgers vector components [$\mathring{A}$] measured in relation to different configurations of crystal lattice.

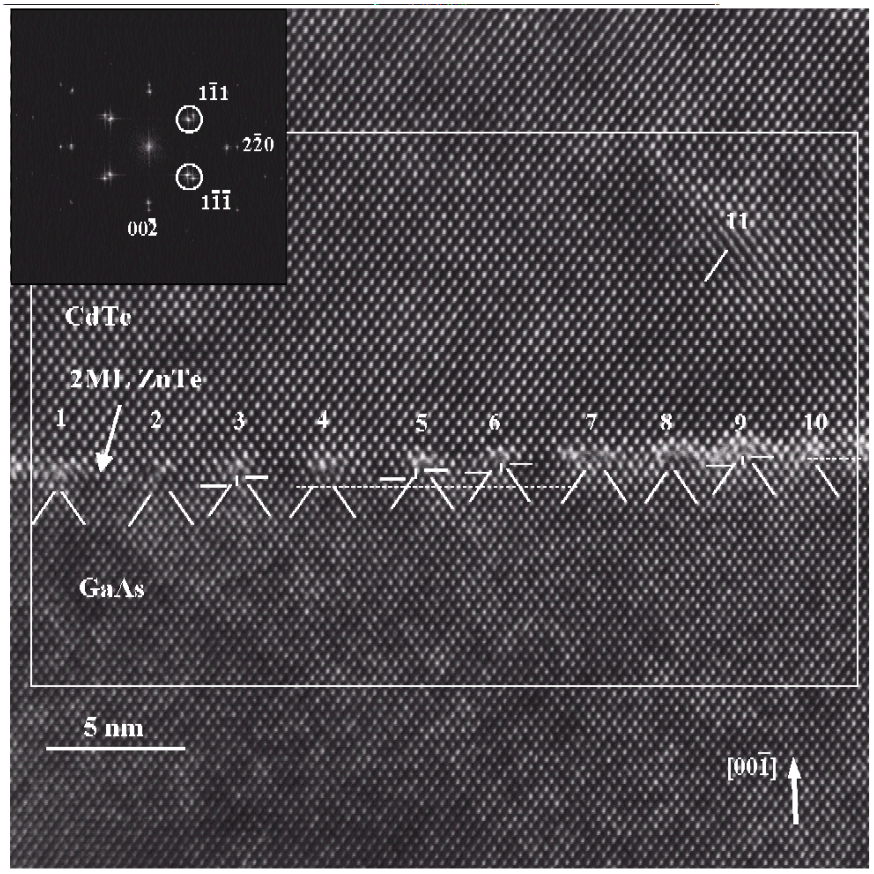

Figure 1: High resolution image of GaAs/ZnTe/CdTe interface observed along the [110] zone axis with its FFT inset.

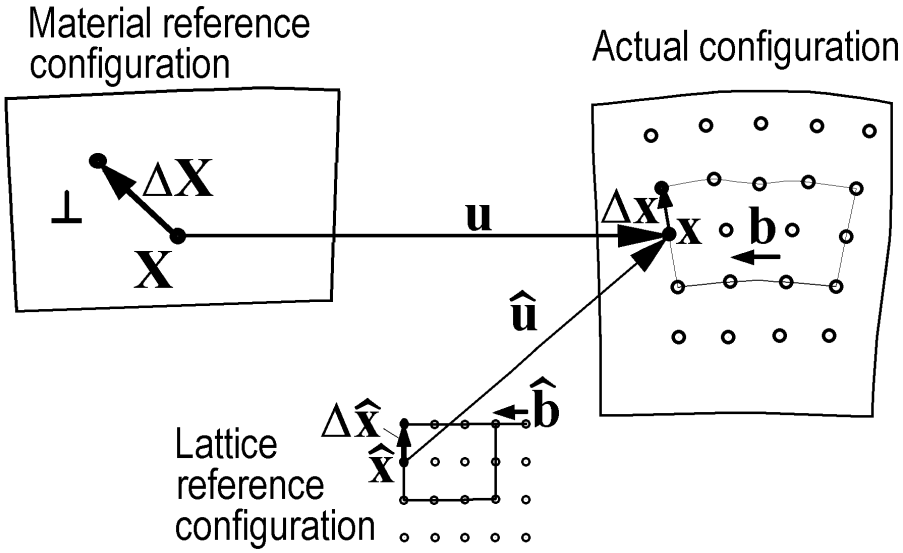

Figure 2: Schematic drawing of configurations considered.

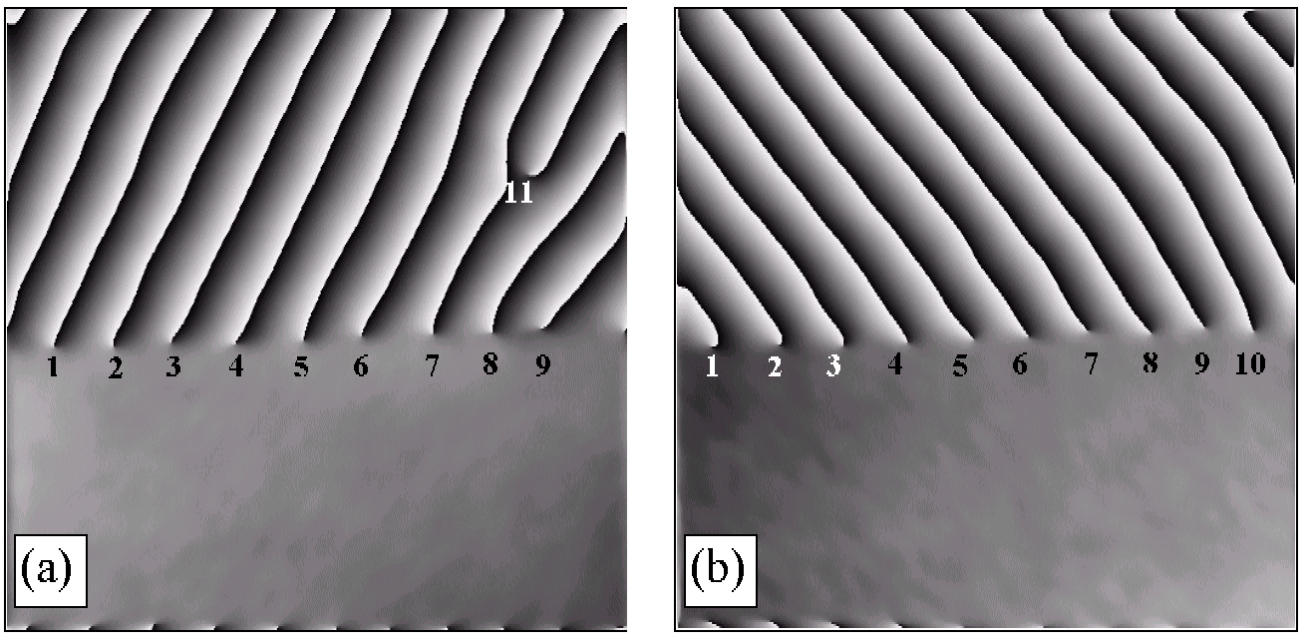

Figure 3: Phase images obtained for reciprocal vectors $\mathbf{g}_{1\bar{1}\bar{1}}$ and $\mathbf{g}_{1\bar{1}1}$ with masks shown in figure 1.

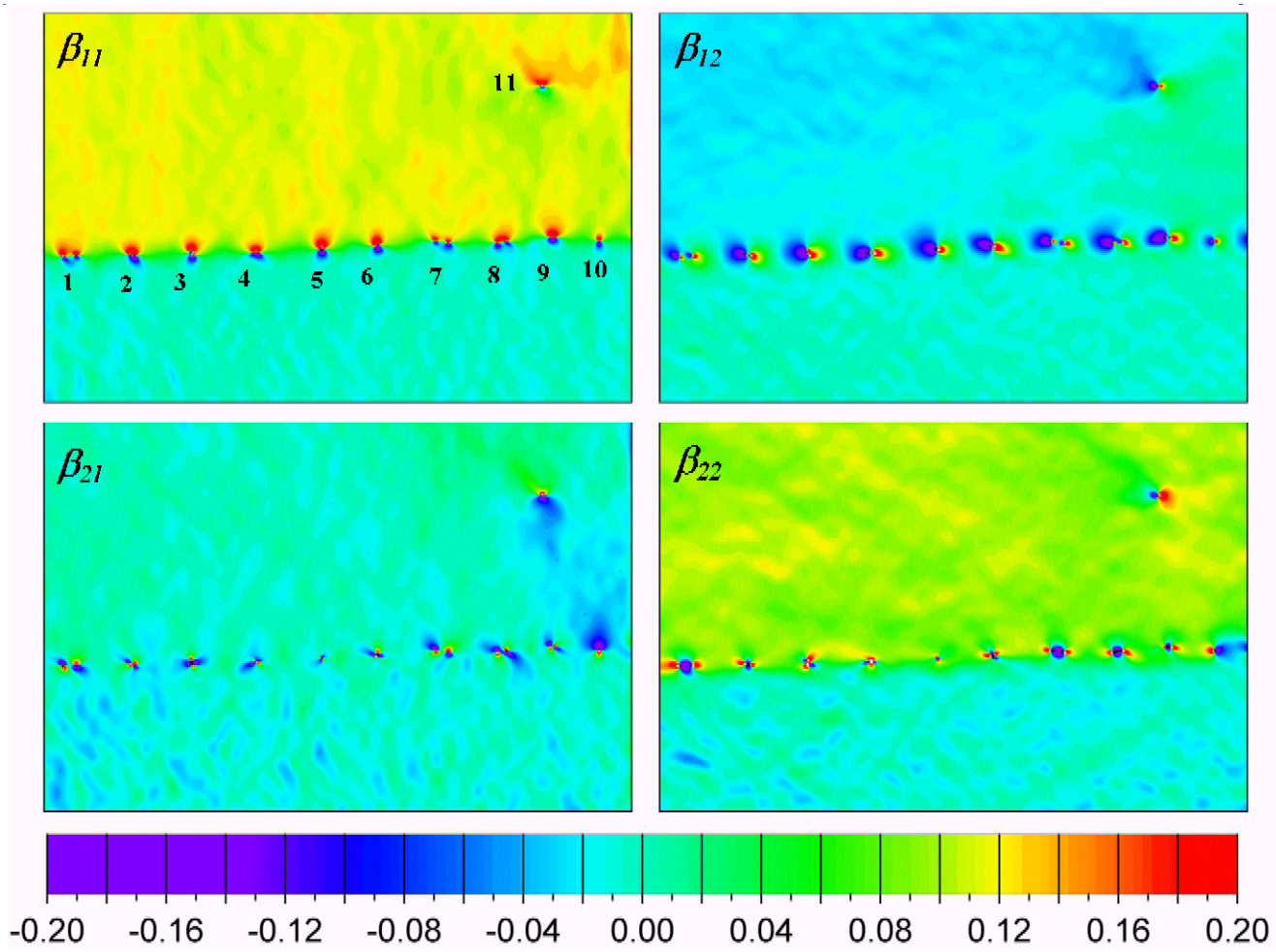

Figure 4: Distribution of lattice distortion tensor $\boldsymbol{\beta}$.

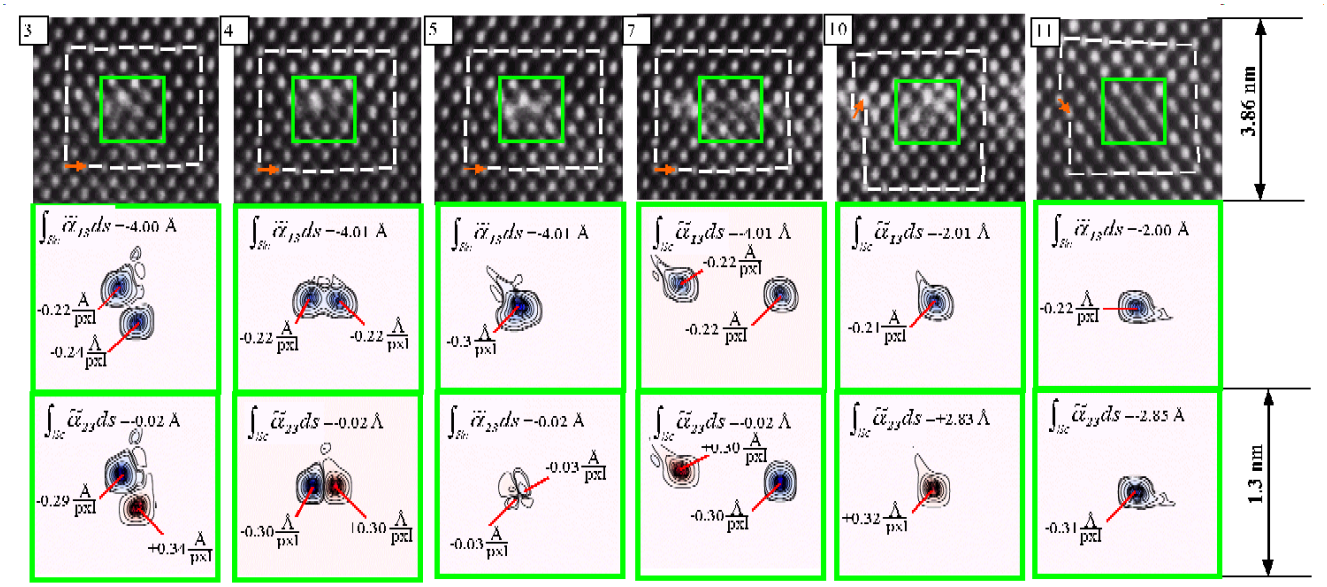

Figure 5: Tensorial distribution of dislocation cores determined from HRTEM micrograph, cf. figure 1.